Electronic Supplementary Material (ESI) for Nanoscale.

Heterostructure CoO-Co_3O_4 nanoparticles anchored on nitrogen-doped hollow carbon spheres as cathode catalysts for Li–O_2 batteries

Lixia Feng, Yongliang Li, Lingna Sun*, Hongwei Mi, Xiangzhong Ren, Peixin Zhang

College of Chemistry and Environmental Engineering, Shenzhen University, Shenzhen, Guangdong 518060, P.R. China

* Corresponding author: Lingna Sun, Tel/Fax: +86-755-26538657, E-mail: lindasun1999@126.com; sunln@szu.edu.cn

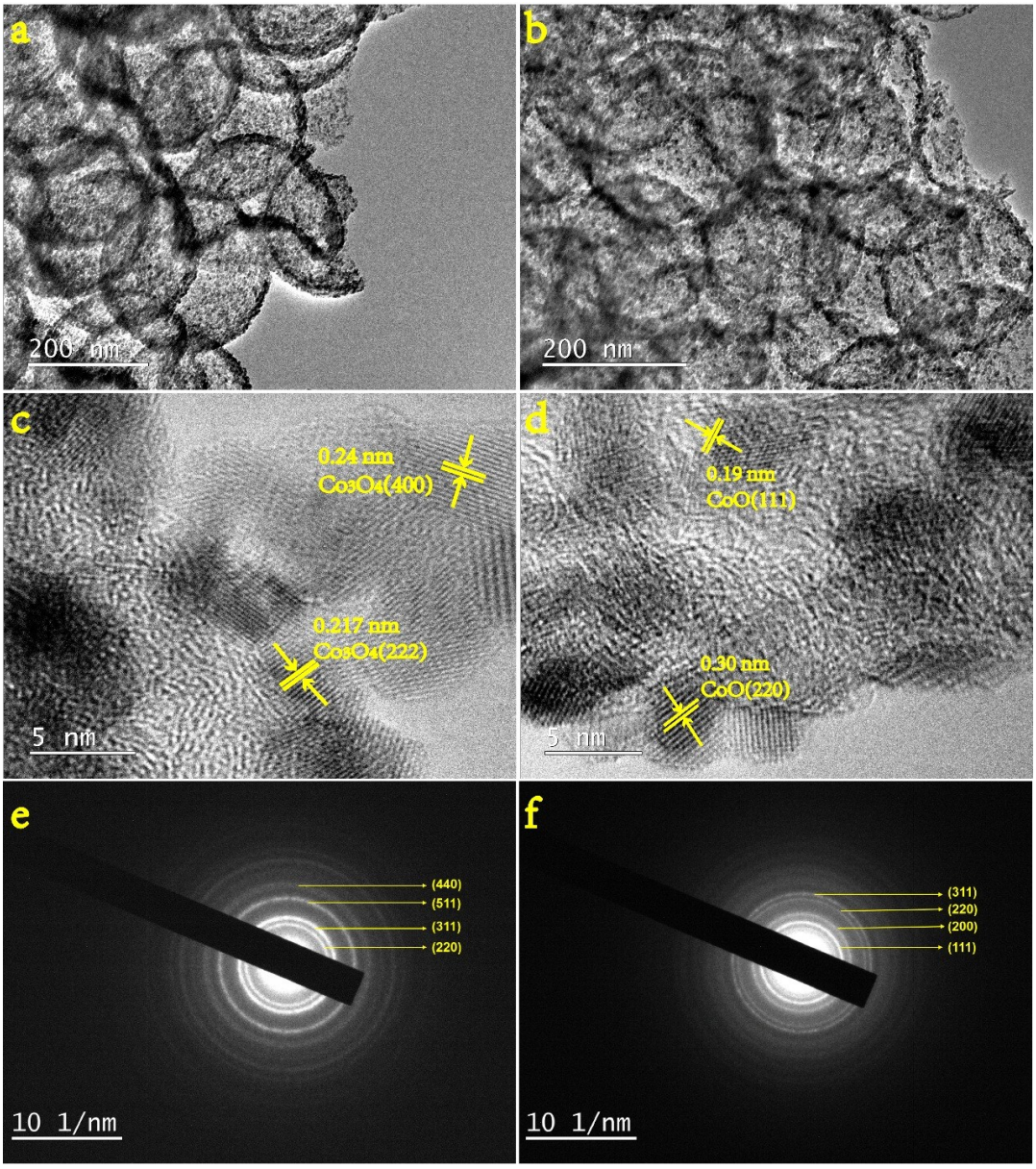

Figure S1. TEM images of (a) N-HC@Co_3O_4 and (b) N-HC@CoO; HRTEM images of (c) N-HC@Co_3O_4 and (d) N-HC@CoO; SAED patterns of (e) N-HC@Co_3O_4 and (f) N-HC@CoO

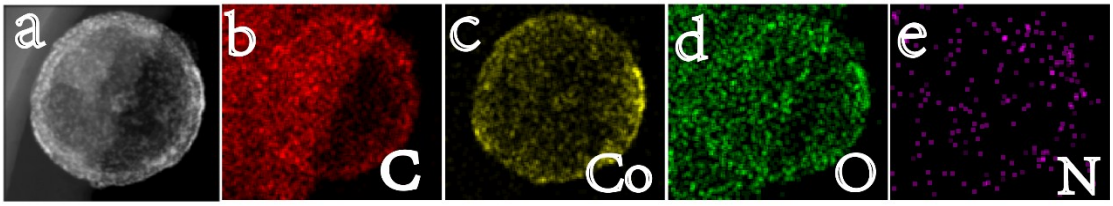

Figure S2. Element present in the N-HC@CoO-Co_3O_4 composite by element mapping of (b) C, (c) Co, (d) O, (e) N

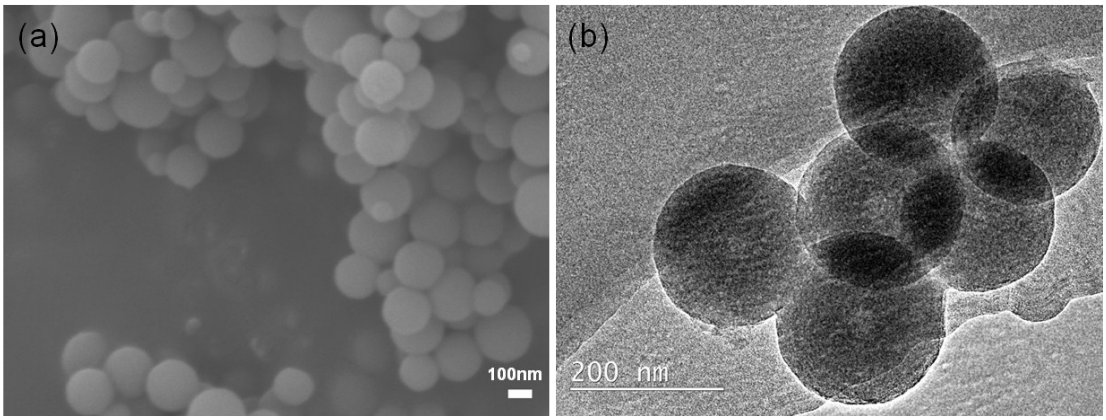

Figure S3. FESEM images of SiO_2@NC (a) and TEM image of SiO_2@NC.

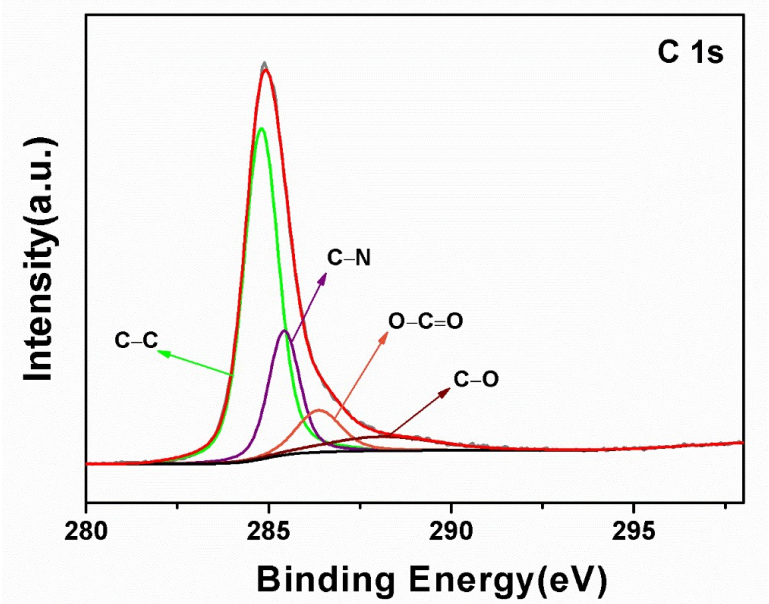

Figure S4. XPS spectrum of the C 1s for the N-HC@CoO-Co_3O_4 composite.

The finely scanned C1s spectrum of N-HC@CoO-Co_3O_4 is shown in Figure S4. Among the four photon energies, the asymmetric C1s spectrum centered at 284.3 eV is C-C group. The peak at 285.6 eV reflects the bonding

structure of the C-N bond, which may be derived from the substitution and defect of the N atom or the edge of the N-HC. The peak at 286.0 eV is attributed to O-C=O group. Due to the higher electronegative N atom, the weakest peak at 288.5 eV is attributed to other binding configurations, such as C-O bond that can form at the N-HC edge. The results show that a large amount of N and O groups are generated on the surface of the N-HC after the calcination treatment.

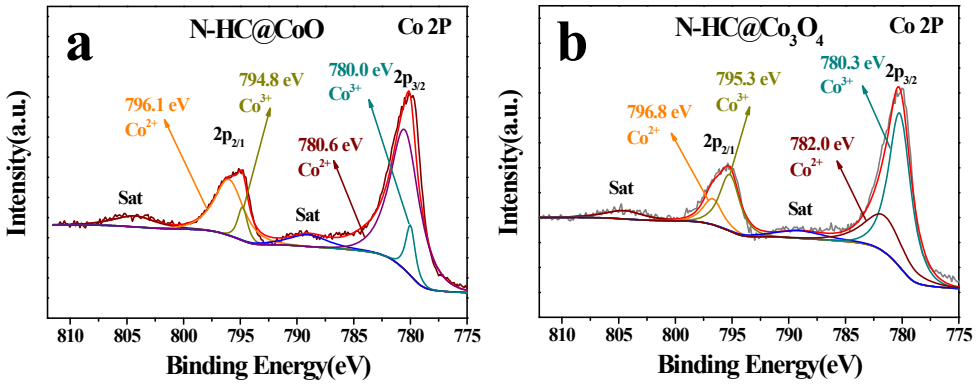

Figure S5. The high-resolution Co 2p XPS spectra for (a) N-HC@CoO and (b) N-HC@Co_3O_4.

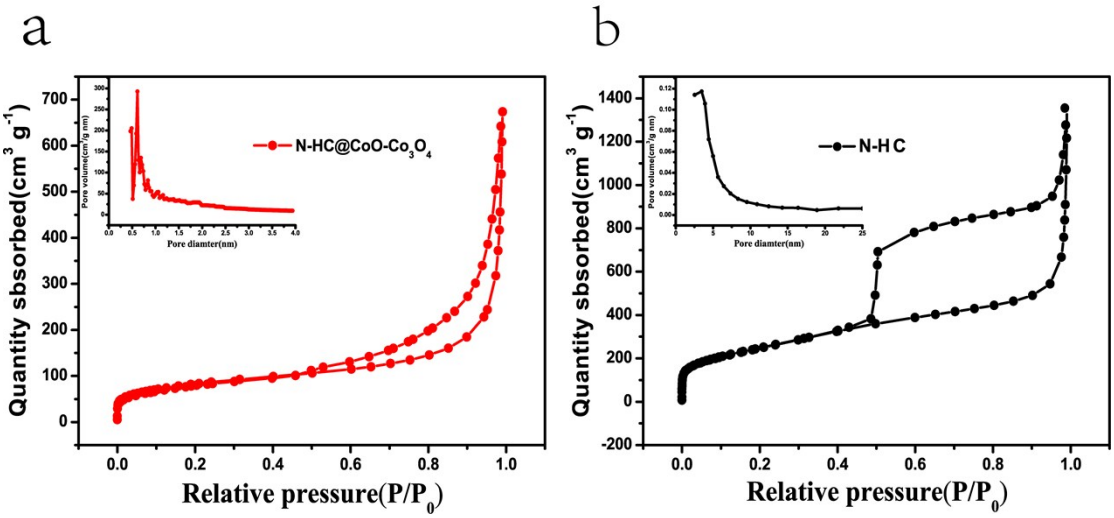

Figure S6. Nitrogen adsorption/desorption isotherm and the corresponding pore size distribution (inset) of N-HC (a) and N-HC@CoO-Co_3O_4 (b).

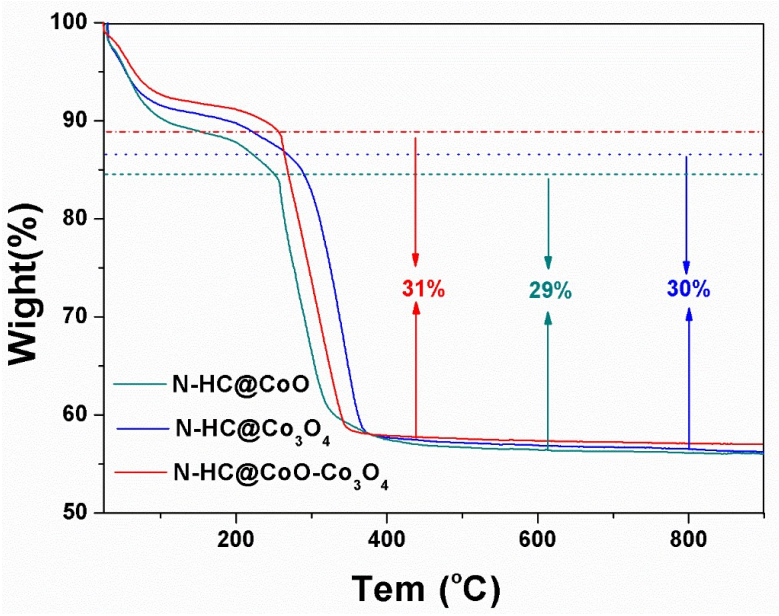

Figure S7. TG curves for different samples under air atmosphere

The TG curves of the three obtained samples are shown in Figure S7. It seems that the trends of mass loss rates in the TG curves are probably the same. At temperature of 0-100°C, the mass reduction is attributed to volatile substances such as water molecules adsorbed on the surface of the sample. The mass loss at around 200-400°C is attributed to the carbon decomposition, which calculated to be around 30wt%.

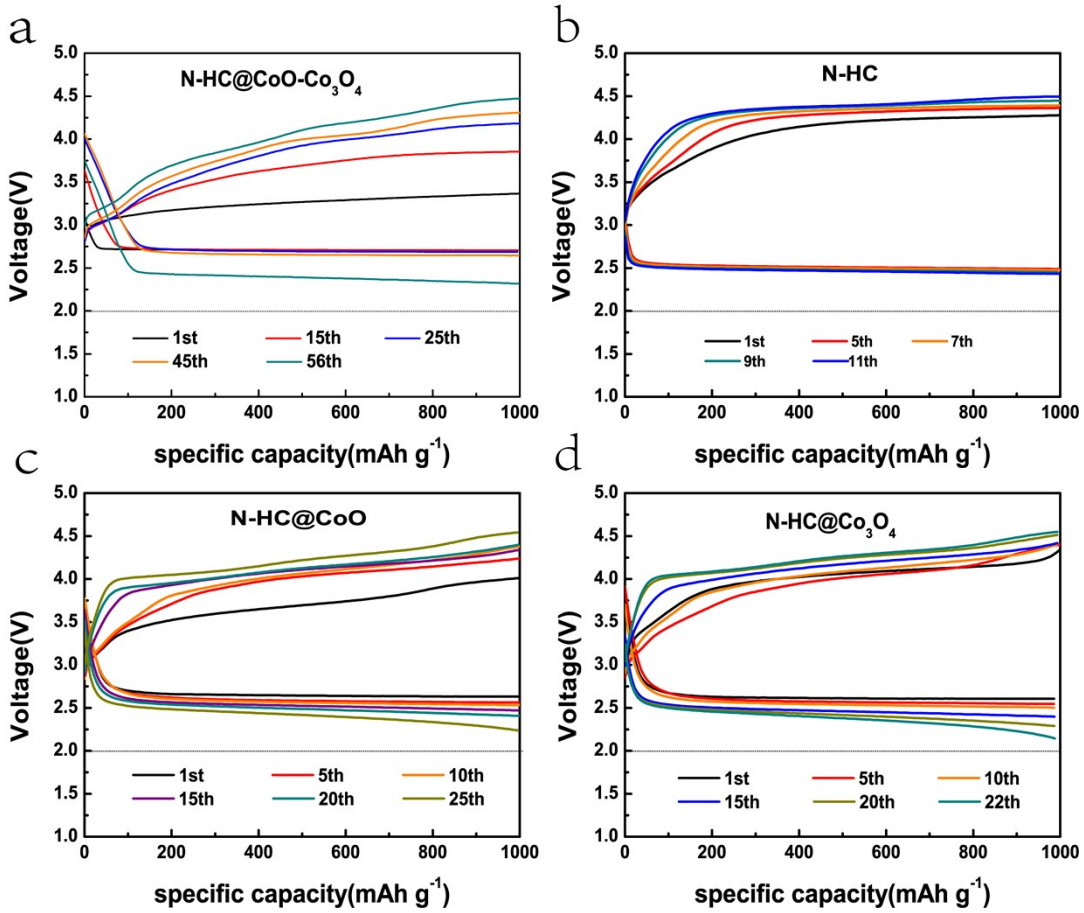

Figure S8. Galvanostatic discharge-charge curves of the N-HC@CoO-Co_3O_4(a), N-HC(b), N-HC@CoO (c) and N-HC@Co_3o_4(d) cathode at various cycles with a capacity limitation of 1000 mAh g^{-1}.

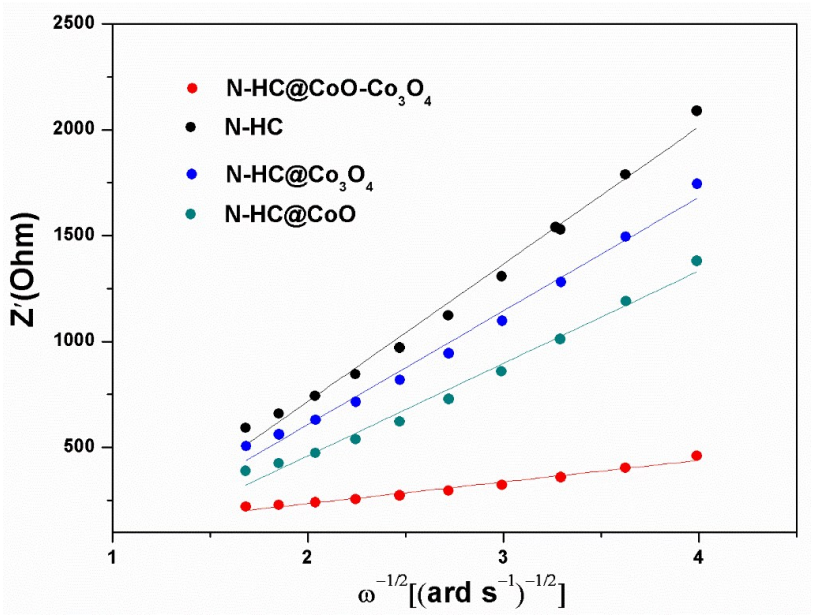

Figure S9. The line relationship of the four cathode materials between Zre and $\omega^{-1/2}$ in the frequency region of 0.1-0.01 Hz

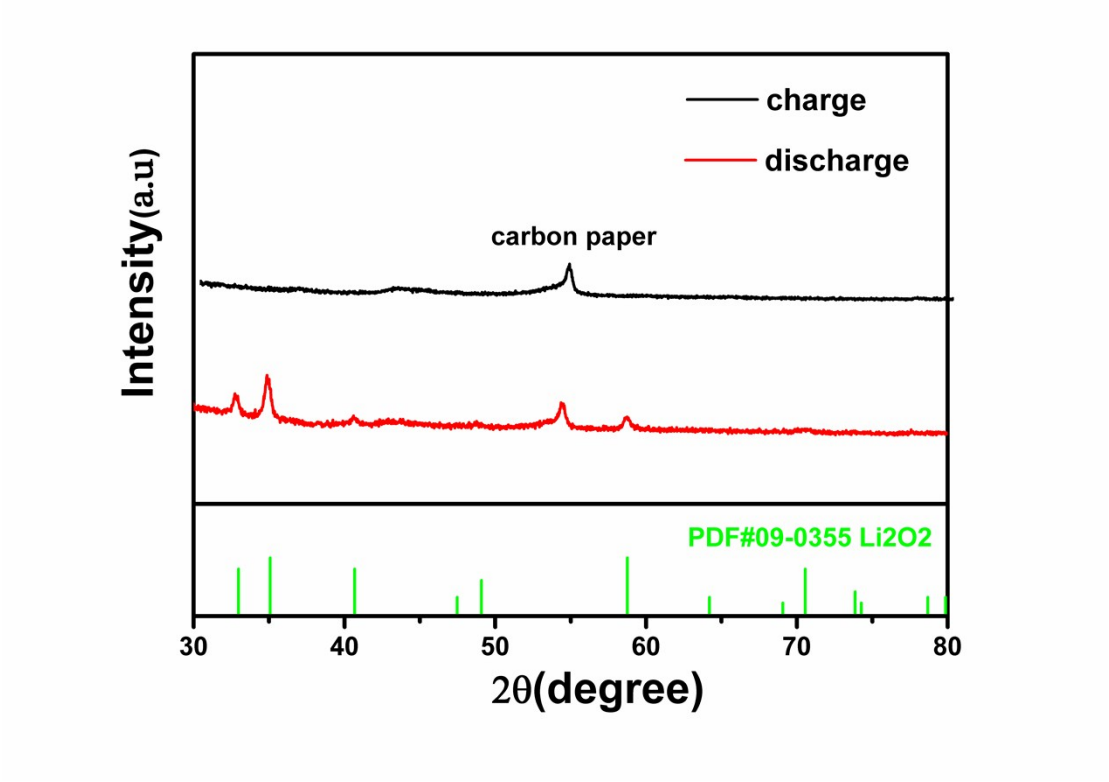

Fig S10. XRD patterns of the N-HC@CoO-Co_3O_4 cathodes at first discharge or charge states

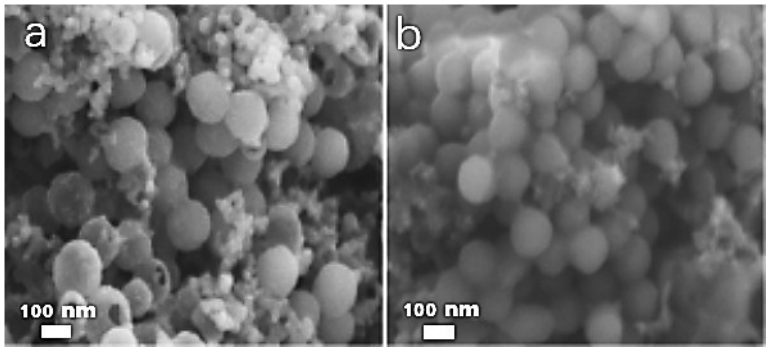

Figure S11. SEM images of the N-HC@CoO-Co_3O_4 after the 20th cycle (a) discharge, (b) recharge.

Figure S11a and b correspond to the SEM images of the discharge and recharge state of the N-HC@CoO-Co_3O_4 cathode after 20th cycle testing at a current density of 300 mA g^{-1} and a limiting capacity of 500 mAh g^{-1}. It can be seen that after several cycles, the spherical structure of N-HC@CoO-Co_3O_4 composite remained very well. It should also be pointed out that the discharged product deposited on its surface could not be ignored, which finally leads to an increase in the overpotential of the battery after 20 cycles (Figure. 4).

Table S1. XPS analysis of composition element content

Element	N-HC	N-HC@CoO-Co_3O_4
	Atomic%	
C	86.29	76.87
Co	--	3.87
O	7.37	15.74
N	5.98	3.61

Table. S2. *R*2, σ and D_{Li+} values determined from the EIS for all the cathodes

	*R*2（Ω）	σ（Ω cm^2 $s^{-0.5}$）	D_{Li+}（cm^2 s^{-1}）
N-HC@CoO-Co_3O_4	60.5	102.05	1.3×10^{-14}
N-HC	177	648.3	3.0×10^{-15}
N-HC@ CoO	68.9	436.49	7.0×10^{-15}
N-HC@Co_3O_4	101.3	596.4	4.0×10^{-15}

Note: R2 represents the resistance of the charge during the transfer process in the electrode material from the equivalent circuit in the main text.

Table S3. Comparison of Li-O_2 battery performance of N-HC@CoO-Co_3O_4 cathode with representative existing cathodes reported in the literature.

Catalyst	Electrolyte	Current Density	Discharge /charge Plateau(V)	Capacity ($mAhg^{-1}$)	Cycles /limit capacity ($mAhg^{-1}$)	Ref.
Co_3O_4nanotube	$LiCF_3SO_3$ /TEGDME	25 mA cm^{-2}	0.99	4299	40/1000	[1]
RuO_2/Co_3O_4 nanowires	$LiPF_6$/ TEGDME	200 mA g^{-1}	1.14	10 850	47/500	[2]
$CoFe_2O_4$/rGO	LiTFSI/ TEGDME	50mAg^{-1}	~1.3	12 235	40/1000	[2]
CoO@Co/C–IL	$LiClO_4$/ DMSO	100 mA g^{-1}	1.11	2660	55/800	[3]
Co_3O_4 nanosheets	LiTFSI/ TEGDME	200 mA g^{-1}	0.9	11 882	80/500 30/1000	[4]
Co-CoO/N-CNR	LiTFSI/ TEGDME	100 mA g^{-1}	1.19	10555	86/1000	[5]
CoO/C	LITFSI/ TEGDME	200 mAg^{-1}	-	5637	50/1000	[6]
RuO_2/La0.6Sr0.4Co0.8Mn0. 2O3 Nanofibers	LiTFSI/ TEGDME	50 mA g^{-1}	1.07	12741.7	100/500	[7]
Co/CNF	LiTFSI/ TEGDME	100 mA g^{-1} 1	0.81	4583	40/500	[8]
N-HC@CoO-Co_3O_4	$LiCF_3SO_3$/ TEGDME	300 mA g^{-1}	0.61	24265	112/500 56/1000	This work

Reference

1. Liu, L.; Guo, H.; Hou, Y.; Wang, J.; Fu, L.; Chen, J.; Liu, H.; Wang, J.; Wu, Y. *Journal of Materials Chemistry A* **2017,** 5, (28), 14673-14681.
2. Cao, Y.; Cai, S. R.; Fan, S. C.; Hu, W. Q.; Zheng, M. S.; Dong, Q. F. *Faraday discussions* **2014,** 172, 215-21.
3. Ni, W.; Liu, S.; Fei, Y.; He, Y.; Ma, X.; Lu, L.; Deng, Y. *Journal of Materials Chemistry A* **2016,** 4, (20), 7746-7753.
4. Wu, F.; Zhang, X.; Zhao, T.; Chen, R.; Ye, Y.; Xie, M.; Li, L. *Journal of Materials Chemistry A* **2015,** 3, (34), 17620-17626.

5. Hyun, S.; Shanmugam, S. *Journal of Power Sources* **2017,** 354, 48-56.
6. Gao, R.; Li, Z.; Zhang, X.; Zhang, J.; Hu, Z.; Liu, X. *ACS Catalysis* **2015,** 6, (1), 400-406.
7. Zhang, X.; Gong, Y.; Li, S.; Sun, C. *ACS Catalysis* **2017,** 7, (11), 7737-7747.
8. Cao, Y.; Lu, H.; Hong, Q.; Bai, J.; Wang, J.; Li, X. *Journal of Power Sources* **2017,** 368, 78-87.